IEEE Access
Multidisciplinary | Rapid Review | Open Access Journal

Received February 3, 2020, accepted February 13, 2020, date of publication February 20, 2020, date of current version March 2, 2020.

Digital Object Identifier 10.1109/ACCESS.2020.2974819

Design and Measurement of an *H*-Band Rectangular TE_{10} to TE_{20} Mode Converter

GUOXIANG SHU[1], (Member, IEEE), ZHENGFANG QIAN[2], AND WENLONG HE[1]

[1]College of Electronics and Information Engineering, Shenzhen University, Shenzhen 518060, China
[2]College of Physics and Photoelectric Engineering, Shenzhen University, Shenzhen 518060, China

Corresponding authors: Guoxiang Shu (gxshu@szu.edu.cn) and Wenlong He (wenlong.he@szu.edu.cn)

This work was supported in part by the National Natural Science Foundation of China under Grant 61901277, in part by the Young Innovative Talents Foundation of Guangdong University under Grant 2018KQNCX215, in part by the Science and Technology Foundation of Shenzhen under Grant JCYJ20180305124406470, and in part by the Natural Science Foundation of Shenzhen University under Grant 2018046.

ABSTRACT A novel methodology of the mode conversion between rectangular TE_{10} and TE_{20} mode based on the *H*-plane T-junction power dividing network is proposed in this paper. A mode converter operating in the *H*-band (220-325 GHz) was analyzed and designed. To decrease the port reflection caused by the T-junction discontinuity, a septum and two symmetric irises were introduced in the converter. Two identical rectangular TE_{20} mode converters joined back-to-back were manufactured by Nano-CNC machining and the electromagnetic properties were measured by using a vector network analyzer. A bandwidth of 228.8-293.1 GHz (64.3 GHz) for transmission coefficient S_{21} around -1.0 dB and port reflection S_{11} around -15.0 dB was measured. The measured results were in good agreement with the simulated ones and manifested high mode conversion efficiency.

INDEX TERMS Rectangular mode converter, H-plane T-junction power dividing network, rectangular TE_{20} mode, high order overmoded slow wave structure.

I. INTRODUCTION

Vacuum electron devices based on high-order overmoded (HOOM) planar slow wave structures (SWSs) are promising terahertz radiation sources due to the large structural dimension, high electron beam current, and high power capacity [1]–[4]. Several kinds of $TE_{20}^{\square}$ mode (here the symbol □ represents the rectangular waveguide) planar SWSs, including a ridge-loaded double staggered grating waveguide [3] and a photonic crystal-loaded folded waveguide [4], have been explored. A $TE_{20}^{\square}$ mode converter, which is used to convert the fundamental $TE_{10}^{\square}$ mode to the desired $TE_{20}^{\square}$ mode, is necessary for the cold test of a $TE_{20}^{\square}$ mode SWS. To accurately measure the electromagnetic properties of the $TE_{20}^{\square}$ mode planar SWS, the $TE_{20}^{\square}$ mode converter should have high mode conversion efficiency, low port reflection, broad frequency bandwidth and flat transmission response. Generally, a good structural performance with compact configuration and easiness of manufacture is also desired. In additional to the aforementioned application in the $TE_{20}^{\square}$ mode planar SWSs, the $TE_{20}^{\square}$ mode converter could also be used as an intermediate transformer in the circular waveguide mode launchers [5]–[7], for instance the Marie-type converter [7]. Furthermore, it could be used in the out-of-phase power dividers [9]–[10].

Several kinds of techniques to excite the $TE_{20}^{\square}$ mode were reported in the previous literatures. (1) One of the classical techniques is by using a mode converter with a 90°-rotation between the wide sides of the input and output waveguides [7]–[9], as shown in Fig. 1(a). The $TE_{10}^{\square}$-$TE_{20}^{\square}$ mode intermediate transformer used in the Marie-type converter adopted such a technique [7]. A *Ka*-band $TE_{01}^{\square}$-$TE_{20}^{\square}$ mode converter based on the similar technique achieved a conversion efficiency of >97.5% in a fractional bandwidth of 30.3% [9]. However, it is not easy for such a technique to extend to higher-order modes. (2) Another common technique to excite the $TE_{20}^{\square}$ mode is by bending the *H*-plane of the input and output rectangular waveguide to a certain angle [10]–[12], as shown in Fig. 1(b). A $TE_{10}^{\square}$-$TE_{20}^{\square}$ mode converter based on an *H*-plane waveguide bend with metallic posts achieved a conversion efficiency of >99% in a fractional bandwidth of ∼12.0% [10]. Two types of $TE_{20}^{\square}$-$TE_{10}^{\square}$ mode converters, based on *H*-plane dual-bend and tri-bend rectangular waveguides, achieved a conversion

The associate editor coordinating the review of this manuscript and approving it for publication was Yongle Wu.

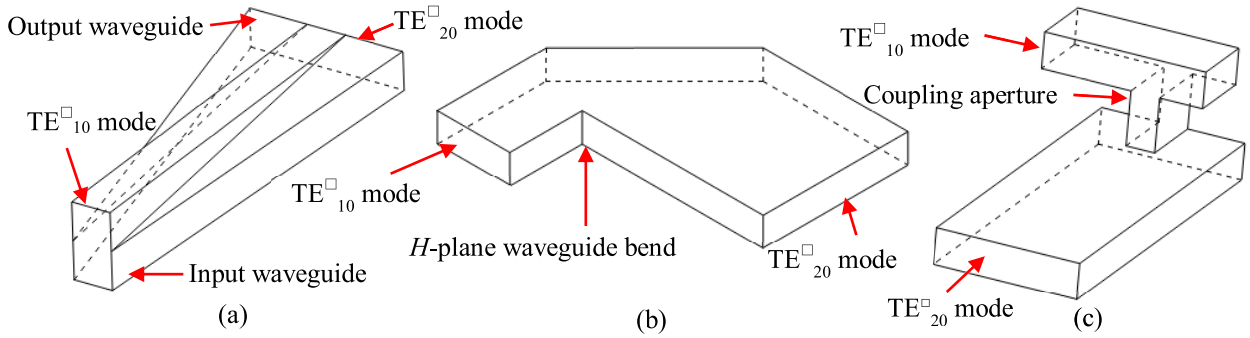

FIGURE 1. Three published configurations of the $TE_{10}^{\square}$-$TE_{20}^{\square}$ mode converter, (a) with a 90°-rotation between the wide sides of the input and output waveguides, (b) based on an *H*-plane waveguide bend, (c) and a coupling aperture.

efficiency of >95% in a fractional bandwidth of 12.8% and 10.3%, respectively [12]. (3) Another methodology to excite the $TE_{20}^{\square}$ mode was based on a coupling aperture [5], [6], as shown in Fig. 1(c). A *Q*-band mode converter based on such a methodology achieved an average mode conversion efficiency of over 97% in a frequency bandwidth of ∼5 GHz, corresponding to a fractional bandwidth of 10.3% [5]. A $TE_{n0}^{\square}$ mode exciter was designed by using a similar methodology [13]. In some instances, it is desired that the input and output ports of the mode converter are aligned on the same axis [14]. Unfortunately, the coupling aperture [5], [6], and *H*-plane waveguide bend [10], [11] based mode converters could not satisfy such a requirement.

In this paper, a novel methodology for the $TE_{10}^{\square}$ to $TE_{20}^{\square}$ mode conversion by using an *H*-plane T-junction is proposed. The rectangular waveguide T-junction is classical in the microwave engineering, which is widely used in many applications, such as the power divider [15], the multiplexer [16], and the feed networks of waveguide antenna arrays [17]. To the best knowledge of the authors, the rectangular waveguide T-junction is for the first time used to construct a mode converter. Such a kind of mode converter possesses several advantages: 1) it could achieve high conversion efficiency and low port reflection in a wide frequency range, 2) it has a relatively compact and easy-to-machine configuration, 3) the center axes of the input and output port are aligned, 4) it is easy for such a structure to extend to higher-order modes. To verify the idea, two identical *H*-band (220-325 GHz) $TE_{20}^{\square}$ mode converters joined back-to-back were machined and measured. Different from the aforementioned mode converters, the mode converter designed in this work operated in the terahertz band rather than the microwave and millimeter-wave band. The geometrical dimensions became smaller with a micrometer-order. A tiny deviation between the machined and designed dimensions would probably worsen the performance of the converter. Consequently, the manufacturing and assembling become increasingly challenging. More importantly, the ohmic loss caused by the surface roughness has a great influence on the transmission efficiency of the terahertz wave. In this paper, the fabrication of a terahertz band $TE_{20}^{\square}$ mode converter was studied.

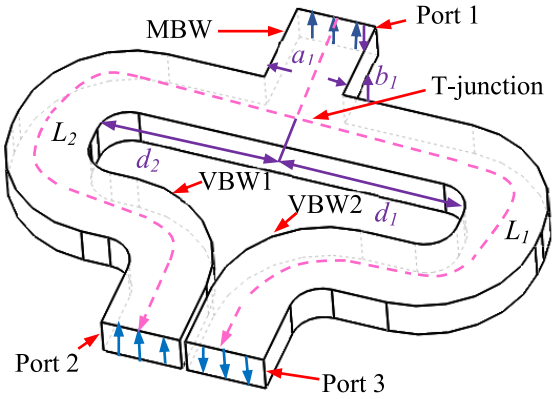

FIGURE 2. A schematic diagram of a 2-way power dividing network based on an *H*-plane T-junction.

The rest of the paper is organized as follows. The mode conversion principle and the design of a $TE_{20}^{\square}$ mode converter are described in section II. Section III presents the machining and measurement of two $TE_{20}^{\square}$ mode converters joined back-to-back and makes discussions of the measured results. Finally, the paper is summarized in section IV.

II. DESIGN AND ANALYSIS

A. THEORETICAL ANALYSIS OF THE MODE CONVERTER

The $TE_{20}^{\square}$ mode converter proposed in this paper is based on a 2-way power dividing network. As shown in Fig. 2, the 2-way power dividing network consisted of a main branch waveguide (MBW), two vice branch waveguides (VBWs), an *H*-plane T-junction and three ports. The cross sectional dimensions of the two VBWs and the MBW are the same. Chamfering of the corners in the VBWs is to reduce the reflection caused by the corner discontinuity.

A few methods for characterizing the rectangular waveguide T-junction have been developed, including the three plane mode-matching technique [16], the boundary-element method [18], and the Y-parameter method [19]. Hence, the theoretical analysis focus on the mode conversion mechanism. To simplify the theoretical analysis, the electromagnetic wave (EM-wave) in the device was assumed to propagate along the central line of the branch waveguide,

as denoted by the dashed curve in Fig. 2. The effect on the phase property from the corner chamfering was neglected. As well known, an obvious difference existing in the $TE_{10}^{\square}$ and $TE_{20}^{\square}$ modes is the number of the half-wavelength standing-wave (1 and 2, respectively). In a $TE_{20}^{\square}$ mode, the two adjacent half-wavelength standing-waves have a property with equal-amplitude and antiphase. Hence, a $TE_{20}^{\square}$ mode converter could be developed from an 2-way power dividing network if the following equations were satisfied.

$$|Pha_2 - Pha_1| = 180^\circ \quad (1)$$

$$Mag_1 - Mag_2 = 0 \quad (2)$$

where Pha_1, Pha_2, Mag_1, and Mag_2 represent the phase and amplitude of the EM-wave propagating through the 1st and 2nd way, respectively. Obviously, a symmetrical H-plane T-junction could achieve outputs with a same phase and amplitude at the two VBWs when an EM-wave signal was injected into the MBW. As the waveguide wavelength λ_g is the same for each branch waveguide, the phase condition expressed in (1) could be realized if the following equations were satisfied.

$$D_{Lp} = |L_2 - L_1| = (2p+1)\frac{\lambda_g}{2} \quad (p = 0,\ 1,\ \ldots) \quad (3)$$

$$\lambda_g = c/(f\sqrt{1-[c/(f\lambda_c)]^2}) \quad (4)$$

$$\lambda_c = 2a_1 (\mathrm{TE}_{10}\ \mathrm{mode}) \quad (5)$$

where, L_1 and L_2 respectively denote the propagation distance of the EM-wave through the 1st and 2nd way. λ_c is the cut off wavelength. a_1 is the wide-side dimension of the waveguide, as shown in Fig. 2. c and f are the velocity of the light in vacuum and the center frequency of the EM-wave, respectively. An overmoded waveguide (OOW) was formed if the two VBMs were joined together at the output port. As a result, the 3-port power dividing network would turn into a 2-port mode converter, and a $TE_{20}^{\square}$ mode could be obtained at the output port if (1)-(2) were satisfied. It should be noted that a $TE_{n0}^{\square}$ ($n = 3, 4, 5\ldots$) mode could also be achieved by using a n-way power dividing network and the theoretical analysis was similar.

B. DESIGN OF AN INITIAL 2-WAY POWER DIVIDING NETWORK BASED ON AN H-PLANE T-JUNCTION

A standard rectangular waveguide (WR-3, 0.864×0.432 mm) was used to construct the MBW and VBWs. Based on (3)-(5), D_{L0} was 0.78 mm in a 2-way power dividing network when f and p in (3) were set to be 0.26 THz and 0, respectively. It could be realized by setting the difference between d_1 and d_2 in Fig. 2 (D_d) to be 0.39 mm.

Based on the aforementioned analysis, an initial 2-way power dividing network was simulated by using the CST-Microwave Studio (CST-MWS) [20], as depicted in the inset of Fig. 3(a). It was shown that it achieved a power dividing with approximately equal amplitude and antiphase over a wide frequency band. As shown in Fig. 3(b), the frequency corresponding to the phase difference between S_{21} and S_{31} of 180° ($f\_{180°}$) was 261.4 GHz when D_d was set to be the designed value, i. e, 0.39 mm. The phase difference versus frequency curve was approximately symmetrical and the phase difference deviated from 180° when the frequency departed from the symmetry center. As shown in Fig. 3(b), the discontinuities of the phase difference versus frequency curve just occurred at the discontinuity frequencies of the phase versus frequency curves of S_{21} and S_{31}. As shown in Fig. 3(c), $f\_{180°}$ was shift with a change of D_d. It was shown that the simulated results were in good agreement with the theoretical analysis.

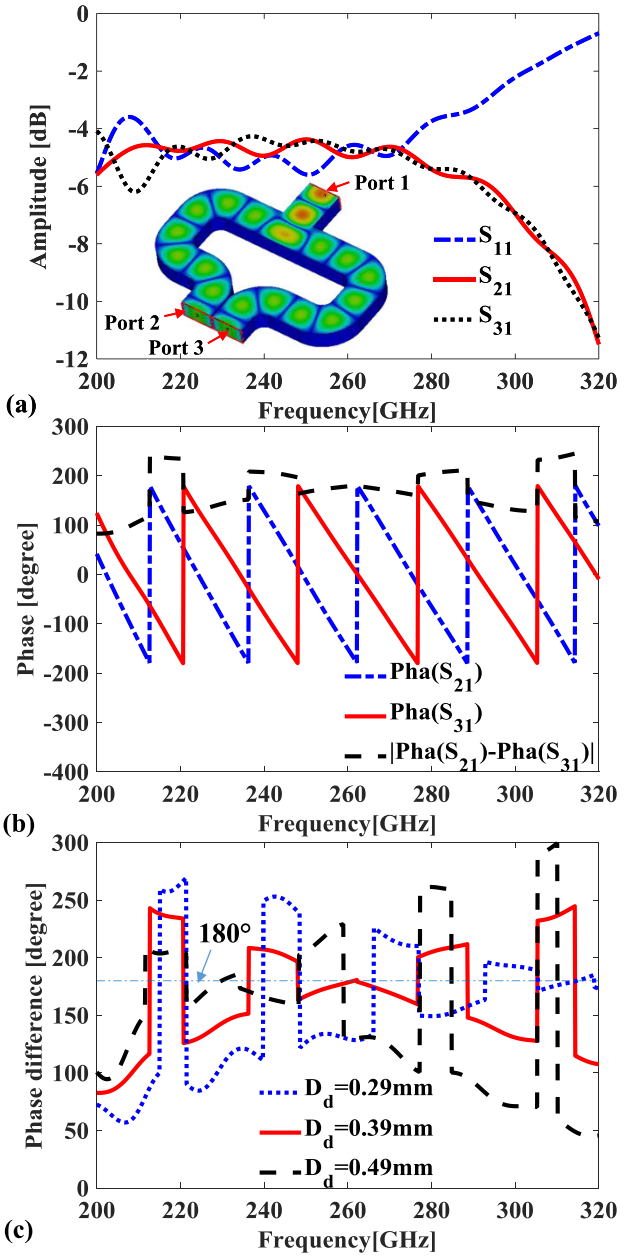

FIGURE 3. (a) Amplitude of the simulated S-parameters for the initial 2-way power dividing network, the inset shows the model with an electric field (*E*-field) distribution at 260 GHz. (b) Phase versus frequency curves for S_{21}, S_{31} and their difference when D_d was 0.39 mm. (c) Phase difference between S_{21} and S_{31} as a function of frequency for the 2-way power dividing networks with different D_d.

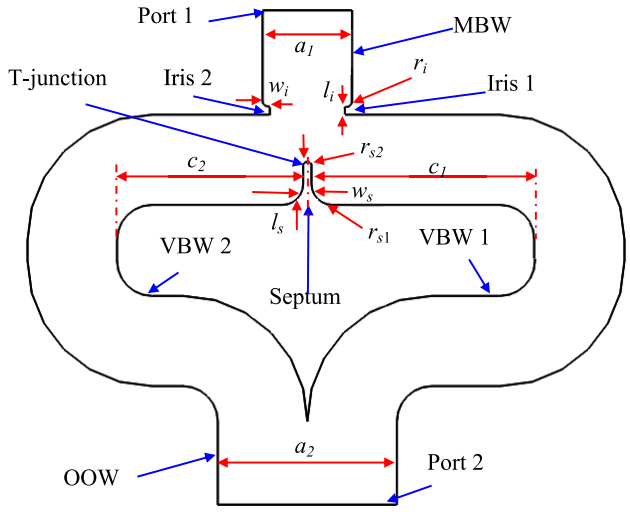

FIGURE 4. A schematic diagram of the $TE_{20}^{\square}$ mode converter with key dimensions.

C. DESIGN OF A $TE_{20}^{\square}$ MODE CONVERTER

An initial $TE_{20}^{\square}$ mode converter was formed when port 2 and 3 of the 2-way power dividing network designed above were combined together. The method of loading septa and irises was widely used to lower the port reflection of the T-junction, [15], [21], [22]. Such a technique was introduced in the design of this mode converter. Irises and septa were intentionally added to introduce additional discontinuities so as to compensate for the discontinuity caused by the T-junction. In the equivalent circuit, they could be equivalent to a reactance, respectively. Finally, an impedance matching of the whole device at the input port was hopeful to be obtained by adjusting the dimensions of the irises and septa. Fig. 4 shows a schematic diagram of the final $TE_{20}^{\square}$ mode converter, which consists of a MBW, an *H*-plane T-junction with two symmetric irises and one septum, two VBWs, an OOW, and two ports. The septum and irises were placed at the center of the T-junction and the end of the MBW, respectively. The heights of the MBW, VBW, OOW, septum and irises were all set to be equal to the height of the standard rectangular waveguide, i. e, 0.432 mm. The chamfering of corners in the septum and irises was also modeled to bring the model closer to the actual fabrication situation. The $TE_{20}^{\square}$ mode converters under three different setups: without any septa and irises, with one septum but without irises, and with one septum and two irises, were individually optimized by using CST-MWS. The sizes of the septum (width w_s, length l_s, chamfering radius r_i) and iris (width w_i, length l_i, chamfering radii r_{s1} and r_{s2}), the length of the auxiliary arms c_1 and c_2 were optimized. The genetic algorithm and interpolated quasi-Newton algorithm were both used for the optimization. Some key optimized dimensions of the final $TE_{20}^{\square}$ mode converter are shown in Table 1.

Fig. 5(a) and (b) show the optimized S-parameters of the $TE_{20}^{\square}$ mode converters under three different setups. It was shown that the initial $TE_{20}^{\square}$ mode converter without any

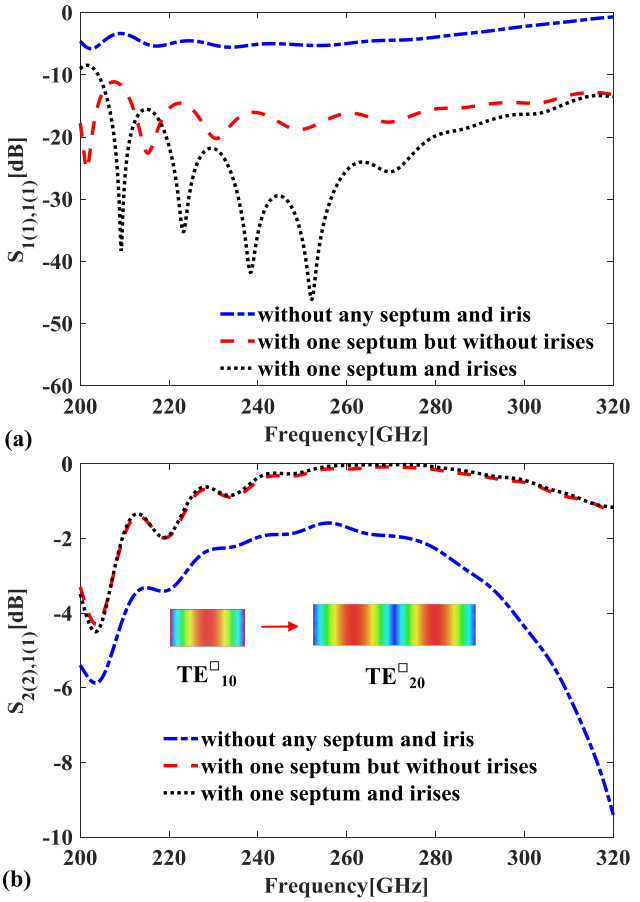

FIGURE 5. Optimized (a) $S_{1(1),1(1)}$ and (b) $S_{2(2),1(1)}$ of the $TE_{20}^{\square}$ mode converters under three different setups. The insets of Fig. 5 (b) give the E-field distribution of $TE_{10}^{\square}$ and $TE_{20}^{\square}$ modes, respectively.

septa and irises could realize the $TE_{10}^{\square}$-$TE_{20}^{\square}$ mode conversion. However, the EM performances were poor, including a high reflection and low conversion coefficient, which was mainly caused by the discontinuity of the *H*-plane T-junction. As shown in Fig. 5(a) and (b), the performances were greatly improved after the introduction of the septum and irises. It was found that the combination of the septum and irises provided more degrees of freedom to achieve an excellent impedance matching. As shown in Fig. 5(a) and (b), the $TE_{20}^{\square}$ mode converter with one septum and two irises achieved better performances in comparison to the one with just one septum. The finally optimized conversion coefficient of the $TE_{20}^{\square}$ mode $S_{2(2),1(1)}$(The number inside the bracket indicates the index *n* in $TE_{n0}^{\square}$ modes) was better than −0.5 dB from 238.6 to 301.4 GHz (62.8 GHz, a fractional bandwidth of 23.2%). The port reflection $S_{1(1),1(1)}$ was lower than −15 dB with a wide frequency bandwidth of 100.2 GHz (39.1% fractional bandwidth) from 206.4-306.7 GHz.

Fig. 6 shows the conversion efficiency of the desired and unwanted modes, which was directly obtained from the transmission coefficient $S_{2(n),1(1)}$ as no EM-wave loss, including the ohmic loss and the EM-wave leakage, was considered in the simulation. The maximum conversion efficiency of

TABLE 1. Optimized dimensions of the final $TE_{20}^{\square}$ mode converter (unit mm).

Iris		w_i	t_i	r_i
		0.07	0.08	0.05
Septum	r_{s1}	r_{s2}	l_s	w_s
	0.2	0.03	0.41	0.08
Rectangular waveguide	c_1	c_2	a_1	a_2
	2.60	2.22	0.864	1.728

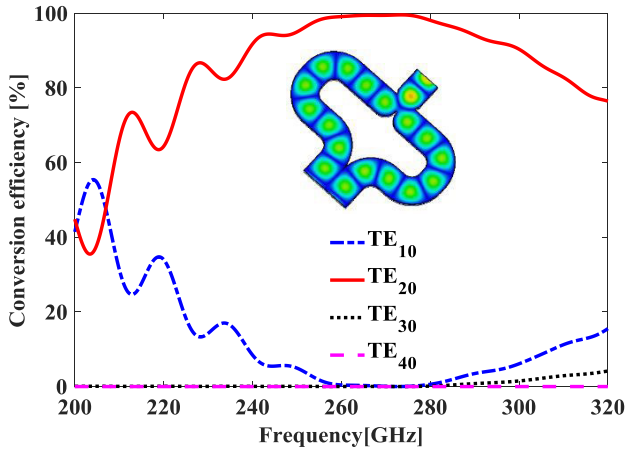

FIGURE 6. Conversion efficiency of the desired and competing modes for the final $TE_{20}^{\square}$ mode converter. The inset gives the simulation model with an E-field distribution at 260 GHz.

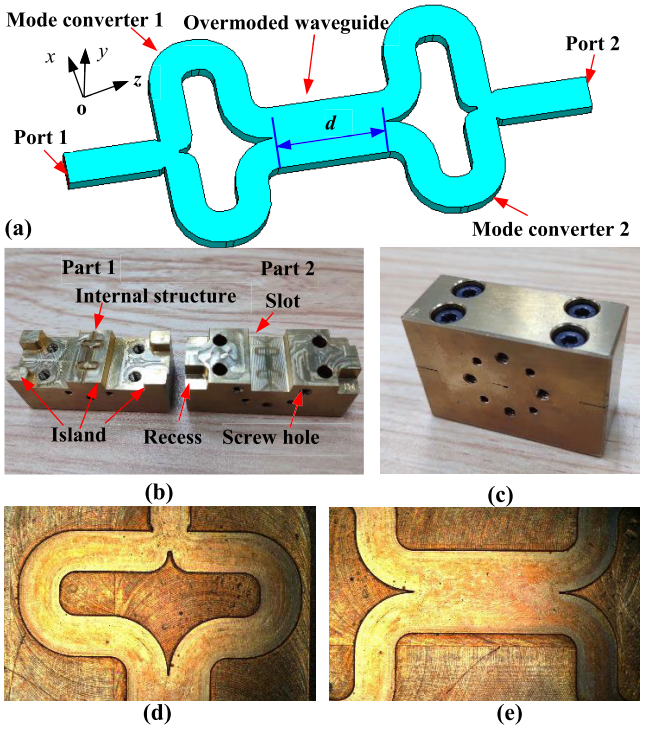

FIGURE 7. (a) A drawing of the fabricated device. Photo of (b) the two parts of the back-to-back joined $TE_{20}^{\square}$ mode converters and (c) the assembled device. Images of (d) the mode converter and (e) overmoded rectangular waveguide observed by an optical microscopy.

99.7% was obtained at 265.9 GHz. Based on the optimized dimensions in Table 1, the theoretical value of the frequency with a maximum conversion efficiency was calculated to be 262.9 GHz by using (3)-(5). Such a 3.0-GHz-shift was acceptable, which was probably attributed to the neglecting of the effects on the phase property from the septum and irises and the chamfering of the corners in the theoretical analysis.

As shown in Fig. 6, the bandwidth for the $TE_{20}^{\square}$-mode conversion efficiency over 95% was up to 37.5 GHz (a fractional bandwidth of 14.0%). The level of the unwanted modes, for instance $TE_{10}^{\square}$, $TE_{30}^{\square}$ and $TE_{40}^{\square}$ mode, were small over that frequency band. When the operating frequency deviated from that frequency band, the $TE_{20}^{\square}$-mode conversion efficiency decreased and the $TE_{10}^{\square}$ mode became the most important competing mode. This was due to the fact that the deviation of the frequency would make the phase difference of the EM-waves in the two VBWs deviate from 180° and approach to 360°. Such a variation trend was in good agreement with the phase difference curve shown in Fig. 3(b). The bandwidth could probably be further improved by introducing a 180 degree phase shifter. However, it would lead to a relatively complicated configuration and thus increase the fabrication difficulties. In this work, a compromise between the electrical and structural performances was made. No 180 degree phase shifters were added in the mode converter as the electrical performances were good enough to realize the cold test of the HOOM planar SWSs.

Table 2 shows the performance comparisons between different methodologies for $TE_{10}^{\square}$-$TE_{20}^{\square}$ mode conversion. The description of the methodologies to excite $TE_{20}^{\square}$ mode in references [5], [9], [10], [12] could be seen in section I of this paper. It could be found that the terahertz band $TE_{20}^{\square}$ mode converters proposed in this paper achieved good electrical and structural performances, including high conversion efficiency, broad frequency bandwidth, compact configuration, planar structure with aligned ports, and good expansibility to higher-order modes.

III. FABRICATION, MEASUREMENT AND DISCUSSION

To verify the methodology and simulations, the back-to-back measurement for the mode converters was used [5], [6], [23], [24]. Two identical $TE_{20}^{\square}$ mode converters joined back-to-back through an overmoded rectangular waveguide were machined from two brass blocks. To reduce the assembling errors, the two converters were machined in one process as shown in Fig. 7(a). The fabricated device consisted of two parts. As shown in Fig. 7(b), the two mode converters were milled at the center of a rectangular alignment island on part 1. Part 2 with a matched rectangular alignment slot was used to cover part 1. The island and slot were designed to precisely mate to each other with very tight tolerances in all dimensions. The alignment island and slot also could prevent the screw holes horizontally located in the waveguide flange being cut in half, thus eliminating a bad junction between the devices and the external rectangular waveguides. To further

TABLE 2. Comparisons of the calculated performances of the $TE_{20}^{\square}$ mode converter proposed in this work and the previously reported references.

Reference	[9]	[10]	[12]	[5]	This work
Frequency band	*Ka*-band	*X*-band	*C*-band /*X*-band	*Q*-band	*H*-band
Basic structure	Input and output waveguide with 90°-rotation	*H*-plane waveguide bend	Dual-bend/tri-bend rectangular waveguides	Coupling aperture	T-junction power dividing network
Fractional bandwidth (Conversion efficiency)	30.3% (>97.5%)	12.0% (>99%)	12.8%(>95%) /10.3%(>95%)	10.3% (> 97%)	14.0% (>95%)
Fractional bandwidth (Return loss)	30.3% (<-15 dB)	~25.4% (<-15 dB)	Not given	~10.3% (<-15 dB)	39.4% (<-15 dB)
Compact	No	Yes	Yes	No	Yes
Aligned	Yes	No	No/Yes	No	Yes
Expansibility	No	Yes	Yes	Yes	Yes

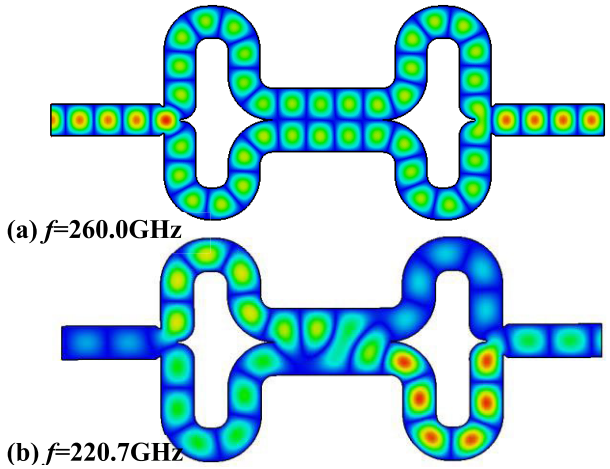

FIGURE 8. *E*-field distribution of the back-to-back joined mode converters observed at (a) 260.0 GHz and (b) 220.7 GHz.

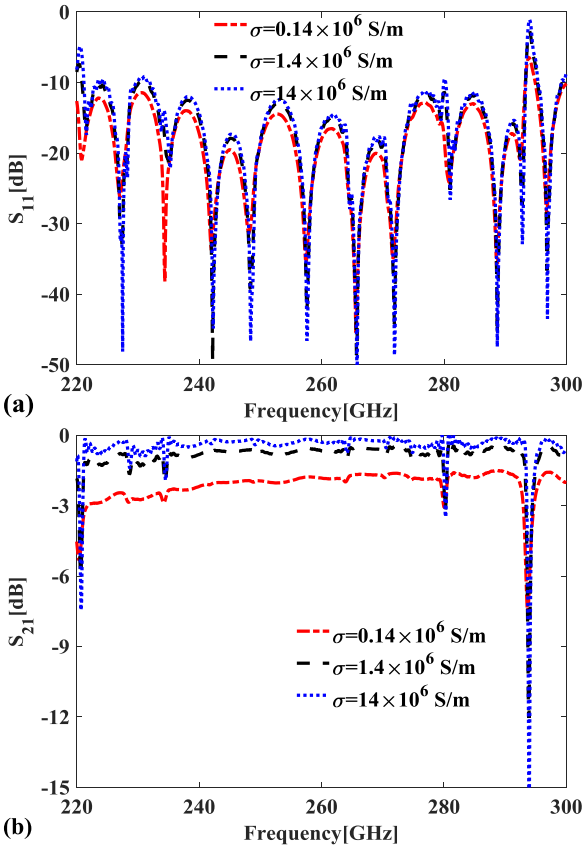

FIGURE 9. Simulated (a) reflection S_{11} and (b) transmission S_{21} of the back-to-back joined mode converters with different conductivity σ of the background material.

reduce the alignment errors, four pairs of small matching rectangular islands and recesses were machined at the four corners of the two parts. To control the dimensions in a small deviation range, the two parts were both milled by a high performance computer numerically controlled (CNC) vertical machining center UVM-450C, which had a maximum rotation speed of 60,000 r/min and could provide a small surface roughness average (R_a) of 40 nm and a high machining accuracy of 2 μm.

As shown in Fig. 7(c), a compact configuration with a size of 38 mm×27 mm×15 mm was achieved for the assembled device. A tight contact between the two parts was observed after the assembly. The images of the mode converters and the overmoded rectangular waveguide observed by an optical microscopy were respectively showed in Fig. 7(d) and (e). It was indicated that a satisfactory machining was obtained.

The ohmic loss caused by the surface roughness was taken into account by introducing the effective conductivity [25]. To estimate the effect on the performance of the back-to-back mode converters from the ohmic loss, the background material was set to be a lossy metal with a variable conductivity σ in the simulation. As shown in Fig 8(a), when a $TE_{10}^{\square}$ mode was input from port 1, it firstly would be converted into $TE_{20}^{\square}$ mode in mode converter 1, and then converted back into $TE_{10}^{\square}$ mode in mode converter 2. As shown in Fig. 9(a), the port reflection S_{11} was almost unchanged when σ varied. However, the value of the transmission coefficient S_{21} would reduce with a decrease of σ denoting a larger ohmic loss, as shown in Fig. 9(b).

Some transmission dips with a narrow bandwidth were observed, peaking at several frequencies, such as 220.7 GHz and 293.9 GHz, as shown in Fig. 9(b). This was probably

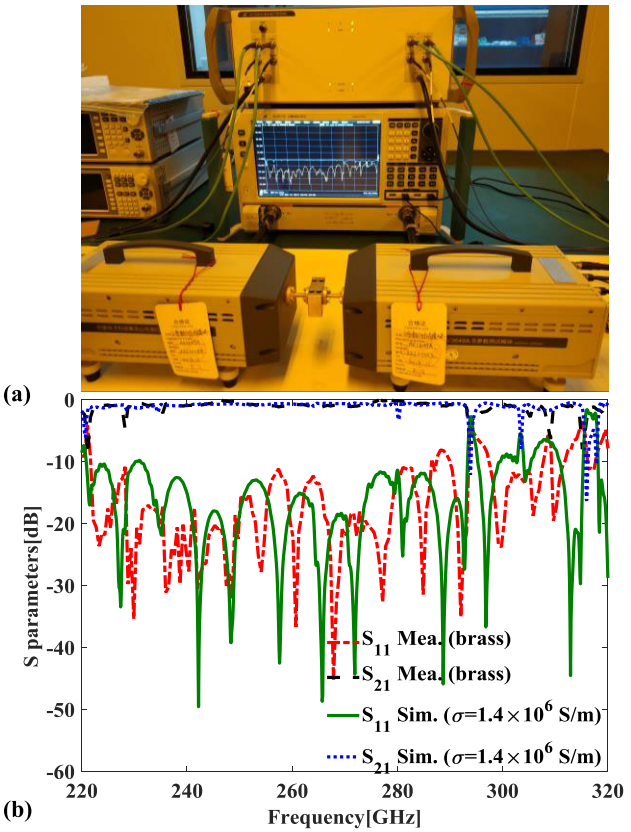

FIGURE 10. (a) VNA measurement setup. (b) Comparisons of the measured and simulated S-parameters.

caused by the possible resonant cavities formed between the two identical converters. As shown in Fig. 8(b), an obvious resonant electric field was observed at 220.7 GHz. The peak level of the transmission dips would reduce when the ohmic loss became larger as illustrated in Fig. 9(b). This was due to the fact that the ohmic loss would decrease the Q-factor of the resonant peak and weaken the resonant electric field. Besides, the transmission dips would shift when changing the distance of the two mode converters d as shown in Fig. 7(a). Such a transmission dip was also found in the measured transmission curve of the back-to-back joined circular waveguide mode converters [5], [6].

A well-calibrated two-port vector network analyzer (VNA) (AV3672E, 10 MHz-67 GHz) connecting with two frequency extenders (AV3649A, 220-325 GHz) was used to measure the S-parameters. As shown in Fig. 10(a), the assembled device was directly connected with the two frequency extenders by two WR-3 flanged rectangular waveguides. Fig. 10(b) makes comparisons of the simulated and measured results of the back-to-back joined mode converters. As shown in Fig. 10(b), the measured S-parameter results were in good agreement with the simulations when σ was set to be 1.4×10^6 S/m. As analyzed above, the measured transmission dips, for instance at 228.3 GHz and 293.7 GHz, were probably caused by the resonance field. S_{21} was around -1.0 dB over the frequency range of 228.8-293.1 GHz (64.3 GHz), corresponding to a fractional bandwidth of 24.6%. S_{11} was around -15.0 dB over that frequency band. It was shown that a good transmission flatness over a wide frequency bandwidth was achieved. Considering the fact that the ohmic loss was high in the terahertz band, the measured transmission coefficient was sufficient to manifest a high mode conversion efficiency. The small deviation between the simulated and measured results was probably caused by the machining and assembling errors.

IV. CONCLUSION

A $TE_{20}^{\square}$ mode converter based on an H-plane T-junction power dividing network was designed and measured in this paper. Measured results agreed well with the simulations. The measured transmission coefficient was higher than -1.0 dB and the port reflection was around -15.0 dB over the frequency range of 228.8-293.1 GHz, indicating a high mode conversion efficiency. Besides, the proposed scheme could be extended to higher-order modes by increasing the ways of the power dividing network. A $TE_{n0}^{\square}$ ($n = 2, 3, \ldots$) mode converter is hopeful to be realized by using an n-way power dividing network. To satisfy the applications with a wider bandwidth requirement, the use of 180 degree phase shifter is a probable method. Studies showed that the proposed methodology was competitive owing to the high conversion efficiency, low reflection, broad bandwidth, and easy-to-fabricate configuration. More importantly, the successful experiment contributed to significant advances of the fabrication of terahertz devices and the research of vacuum electron devices based on HOOM SWSs.

REFERENCES

[1] A. Gee and Y.-M. Shin, "Gain analysis of higher-order-mode amplification in a dielectric-implanted multi-beam traveling wave structure," *Phys. Plasmas*, vol. 20, no. 7, pp. 073106–1–073106–7, Jul. 2013.
[2] G. X. Shu, G. Liu, and Z. F. Qian, "Simulation study of a high-order mode terahertz radiation source based on an orthogonal grating waveguide and multiple sheet electron beams," *Opt. Express*, vol. 26, no. 7, pp. 8040–8048, Mar. 2018.
[3] G. Shu, G. Liu, L. Chen, H. Bambarandage, and Z. Qian, "Terahertz backward wave radiation from the interaction of high-order mode and double sheet electron beams," *J. Phys. D, Appl. Phys.*, vol. 51, no. 5, Jan. 2018, Art. no. 055107.
[4] N. Shi, H. Wang, D. Xu, Z. Wang, Z. Lu, H. Gong, D. Liu, Z. Duan, Y. Wei, and Y. Gong, "Study of 220 GHz dual-beam overmoded photonic crystal-loaded folded waveguide TWT," *IEEE Trans. Plasma Sci.*, vol. 47, no. 6, pp. 2971–2978, Jun. 2019.
[5] G. Liu, Y. Wang, Y. Pu, and Y. Luo, "Design and microwave measurement of a novel compact $TE_{0n}/TE_{1n'}$-Mode converter," *IEEE Trans. Microw. Theory Tech.*, vol. 64, no. 12, pp. 4108–4116, Sep. 2016.
[6] Y. Wang, L. Wang, G. Liu, G. Shu, K. Dong, J. Wang, R. Yan, H. Fu, Y. Yao, Y. Luo, and S. Wang, "Wideband circular TE_{21} and TE_{01} mode converters with same exciting topologies," *IEEE Trans. Electron Devices*, vol. 63, no. 12, pp. 4955–4960, Oct. 2016.
[7] S. S. Saad, J. B. Davies, and O. J. Davies, "Analysis and design of a circular TE_{01} mode transducer," *IEE J. Microw., Opt. Acoust.*, vol. 1, no. 2, pp. 58–62, Jan. 1977.
[8] Y. Xu, T. Peng, M. Sun, Y. Luo, J. Wang, W. Jiang, G. Liu, and Z. Wu, "Design and test of broadband rectangular waveguide TE_{10} to circular waveguide TE_{21} and TE_{01} mode converters," *IEEE Trans. Electron Devices*, vol. 66, no. 8, pp. 3573–3579, Aug. 2019.
[9] P. Zhao, Q. Wang, and J. Deng, "A novel broadband rectangular waveguide TE_{01}-TE_{20} mode converter," *IEEE Microw. Wireless Compon. Lett.*, vol. 28, no. 9, pp. 747–749, Sep. 2018.

[10] S. Matsumoto, I. Ohta, K. Fukada, T. Kawai, K. Iio, and T. Kashiwa, "A TE_{10}-TE_{20} mode transducer utilizing a right-angled corner and its application to a compact H-plane out-of-phase power divider," in *Proc. Asia Pacific Microw. Conf.*, Singapore, Dec. 2009, pp. 1008–1011.
[11] A. A. Kirilenko, L. A. Rud, and V. I. Tkachenko, "Nonsymmetrical *H*-plane corners for TE_{10}-TE_{q0}-mode conversion in rectangular waveguides," *IEEE Trans. Microw. Theory Tech.*, vol. 54, no. 6, pp. 2471–2477, Jun. 2006.
[12] Q. Zhang, C.-W. Yuan, and L. Liu, "Theoretical design and analysis for TE_{20}-TE_{10} rectangular waveguide mode converters," *IEEE Trans. Microw. Theory Techn.*, vol. 60, no. 4, pp. 1018–1026, Apr. 2012.
[13] Y. L. Yao, J. X. Wang, and H. Li, "Broadband rectangular TE_{n0} mode exciter with H-plane power dividers for 100 GHz confocal gyro-devices," *Rev. Sci. Instrum*, vol. 88, no. 7, pp: 074701–1-074701–5, 2017.
[14] Q. Zhang, C. W. Yuan, and L. Liu, "TM_{01}-TE_{11} mode converter of tri-bend circular waveguides," *High Power Laser Part. Beams*, vol. 20, no. 7, pp. 1173–1176, 2008.
[15] S. H. Lee, J. S. Kim, Y. J. Yoon, and W. S. Lee, "Six-way power divider for series feed using H-plane T-junctions," *Microw. Opt. Technol. Letters*, vol. 58, no. 7, pp. 1622–1626, Apr. 2016.
[16] X.-P. Liang, K. A. Zaki, and A. E. Atia, "A rigorous three plane mode-matching technique for characterizing waveguide T-junctions, and its application in multiplexer design," *IEEE Trans. Microw. Theory Techn.*, vol. 39, no. 12, pp. 2138–2147, Dec. 1991.
[17] G.-L. Huang, S.-G. Zhou, T.-H. Chio, H.-T. Hui, and T.-S. Yeo, "A low profile and low sidelobe wideband slot antenna array feb by an amplitude-tapering waveguide feed-network," *IEEE Trans. Antennas Propag.*, vol. 63, no. 1, pp. 419–423, Jan. 2015.
[18] M. Koshiba and M. Suzuki, "Application of the boundary-element method to waveguide discontinuities," *IEEE Trans. Microw. Theory Tech.*, vol. 34, vol. 2, pp. 301–307, Feb. 1986.
[19] E. D. Sharp, "An exact calculation for a T-junction of rectangular waveguides having arbitrary cross sections," *IEEE Trans. Microw. Theory Techn.*, vol. MTT-15, no. 2, pp. 109–116, Feb. 1967.
[20] *CST-Computer Simulation Technology*. Accessed: Jun. 2019. [Online]. Available: http://www.cst.com/products/cstmws
[21] S. Yang and A. E. Fathy, "Synthesis of a compound T-junction for a two-way splitter with arbitrary power ratio," in *IEEE MTT-S Int. Microw. Symp. Dig.*, Jun. 2005, pp. 1–4.
[22] J. H. Bang, S. M. Hwang, S. G. Lee, and B. C. Ahn, "Design formulas for the H-plane septum power divider in a rectangular waveguide," *Microw. Opt. Technol. Lett.* vol. 37, no. 5, pp. 390–393, Jun. 2003.
[23] X. Cui, G. Wang, T. Jiang, H. Shao, J. Sun, X. Wu, X. Bai, X. Zhang, and Z. Zhang, "High-efficiency, broadband converter from a rectangular waveguide TE_{10} mode to a circular waveguide TM_{01} mode for overmoded device measurement," *IEEE Access*, vol. 6, pp. 14996–15003, Mar. 2018.
[24] T.-H. Chang, C.-H. Li, C.-N. Wu, and C.-F. Yu, "Generating pure circular TE_{mn} modes using Y-type power dividers," *IEEE Trans. Microw. Theory Techn.*, vol. 58, no. 6, pp. 1543–1550, Jun. 2010.
[25] M. P. Kirley and J. H. Booske, "Terahertz conductivity of copper surfaces," *IEEE Trans. THz Sci. Technol.*, vol. 5, no. 6, pp. 1012–1020, Nov. 2015.

GUOXIANG SHU (Member, IEEE) received the Ph.D. degree from the University of Electronic Science and Technology of China, Chengdu, China, in 2017. He was a Visiting Researcher with the University of Strathclyde, U.K. Since September 2017, he has been an Assistant Professor with the College of Electronics and Information Engineering, Shenzhen University, China. He has been recognized as the Shenzhen Overseas High-level Talents. He has authored/coauthored over 50 technical publications. His research interests include sheet electron beam TWTs, BWOs and EIOs, pseudospark-sourced electron beam devices, millimeter-wave dielectric measurement, and passive devices (couplers, mode convertors, and resonant cavities).

ZHENGFANG QIAN received the Ph.D. degree from Chongqing University, Chongqing, China, in 1991. Since 2016, he has been the Chair Professor with the College of Physics and Photoelectric Engineering, Shenzhen University, Shenzhen, China. His current research areas focus on nanostructured antennas, terahertz antennas, and smart antennas as well as wireless sensors and communications.

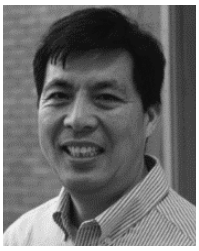

WENLONG HE received the Ph.D. degree in relativistic electron beams and masers from the University of Strathclyde, Glasgow, U.K., in 1995. He was a Senior Research Fellow with the Scottish Universities Physics Alliance, Department of Physics, University of Strathclyde. Since November 2018, he has been the Chair Professor with the College of Electronics and Information Engineering, Shenzhen University, China. His main research interests include relativistic electron beams, gyrotron traveling-wave amplifier (gyro-TWA)/backward-wave oscillators, cyclotron auto-resonance masers (CARMs), free-electron lasers (FELs), and other high-power microwave and terahertz devices.